$(Fe_{1-x}Ni_x)_5GeTe_2$: An antiferromagnetic triangular Ising lattice with itinerant magnetism

Xunwu Hu, Dao-Xin Yao,* and Kun Cao†

Center for Neutron Science and Technology, Guangdong Provincial Key Laboratory of Magnetoelectric Physics and Devices, State Key Laboratory of Optoelectronic Materials and Technologies, School of Physics, Sun Yat-Sen University, Guangzhou, 510275, China

(Received 21 September 2022; revised 15 November 2022; accepted 12 December 2022; published 23 December 2022; corrected 5 January 2023)

Based on first-principles calculations, an antiferromagnetic Ising model on a triangular lattice has been proposed to interpret the order of Fe(1)-Ge pairs and the formation of $\sqrt{3} \times \sqrt{3}$ superstructures in the Fe_5GeTe_2 (F5GT) as well as to predict the existence of similar superstructures in Ni doped F5GT (Ni-F5GT). Our paper suggests that F5GT systems may be considered as a rare structural realization of the well-known antiferromagnetic Ising model on a triangular lattice. Based on the superstructures, a Heisenberg-Landau Hamiltonian, taking into account longitudinal spin fluctuations, is implemented to describe magnetism in both F5GT and Ni-F5GT. We unveil that frustrated magnetic interactions associated with Fe(1), tuned by a tiny Ni doping, is responsible for the experimentally observed enhancement of the T_c to 478 K in Ni-F5GT. Itinerant magnetism, reflected by longitudinal spin fluctuations, are found to only affect the T_c's mildly with a modification of ∼5% with respect to that obtained with standard Heisenberg interactions. Our calculations show that at low doping levels, monolayer Ni-F5GT has almost the same magnetic phase diagram as that of the bulk, which indicates a pervasive beyond room-temperature ferromagnetism in this Ni-doped two-dimensional system.

DOI: 10.1103/PhysRevB.106.224423

I. INTRODUCTION

In recent years, quasi-two-dimensional (quasi-2D) van der Waals ferromagnetic (FM) materials, such as $Cr_2Ge_2Te_6$ [1], CrI_3 [2], $CrTe_2$ [3,4] and Fe_nGeTe_2 ($n = 3$–5) [5–9], have garnered significant attention due to their novel physical properties and potential applications in spintronic devices. Among them, Fe_5GeTe_2 (F5GT) system is particularly attractive, owing to its extraordinary properties suitable for practical applications, including metallic ferromagnetism with near room-temperature T_c (279–332 K), large saturation moment (1.8–2.1 μ_B/Fe) [7,8,10–12] and high tunability of chemical compositions [8,13–16]. More recently, Chen *et al.* reported that, by 36% Ni doping in the F5GT compound, its T_c can be significantly enhanced to 478 K [14]. They further postulated that this enhancement of T_c in Ni-doped F5GT (Ni-F5GT) may be caused by increased magnetic exchange interactions due to the structural alterations.

On the other hand, one extraordinary characteristic of the F5GT systems is that there are two split sites of Fe positions, labeled here as $Fe(1)_{up}$ and $Fe(1)_{dn}$ with only one position occupiable within each $Fe(1)_{up}$, $Fe(1)_{dn}$ pair, leading to intrinsic structural disorders [7]. Due to the difficulty of dealing with disorders, so far, most theoretical studies are based on an ordered lattice structure with fully occupied $Fe(1)_{up}$ (uuu) or $Fe(1)_{dn}$ (ddd) positions [16–20]. Intriguingly, scanning tunneling microscopy experiments indicate that the F5GT compound has ordered $\sqrt{3} \times \sqrt{3}$ superstructures driven by the ordering of Fe(1) atoms [21,22]. It is then natural to suspect that lattice structural details may have subtle interplay with magnetic ordering in both F5GT and Ni-F5GT, and the $\sqrt{3} \times \sqrt{3}$ superstructures could be more representable to the true experimental lattice structures. Ershadrad *et al.* investigated the structural ordering of F5GT based on *ab initio* calculated energies [23] but ignored the effect from temperature and entropy. Therefore, the mechanism behind the formation of the $\sqrt{3} \times \sqrt{3}$ superstructures and their interplay with magnetic ordering especially the itinerant magnetism and high T_c's, remain elusive.

In this paper, we propose an antiferromagnetic Ising model on a triangular lattice, based on first-principles calculations, to interpret the ordering of Fe(1) atoms and the formation of the $\sqrt{3} \times \sqrt{3}$ superstructures in F5GT. Similar superstructures are then predicted to exist in Ni-F5GT. Our paper suggests that F5GT systems may be considered as a rare structural realization of the well-known antiferromagnetic Ising model on a triangular lattice. Based on the superstructures, a Heisenberg-Landau Hamiltonian, taking into account Heisenberg exchange interactions and longitudinal spin fluctuations, is implemented to study the magnetic properties of F5GT and Ni-F5GT. We unveil that frustrated magnetic interactions associated with Fe(1), tuned by a tiny Ni doping, is responsible for the experimentally observed significant enhancement of the T_c in Ni-F5GT. In contrast, calculated results based on the uuu structure deviate qualitatively from experiments. Itinerant magnetism, reflected by longitudinal spin fluctuations, are found to only affect the T_c's mildly, with a modification of ∼5% with respect to that obtained with standard Heisenberg interactions. Our calculations further show that at low doping levels, the magnetic behaviors of the monolayer Ni-F5GT

*yaodaox@mail.sysu.edu.cn
†caok7@mail.sysu.edu.cn

 ©2022 American Physical Society

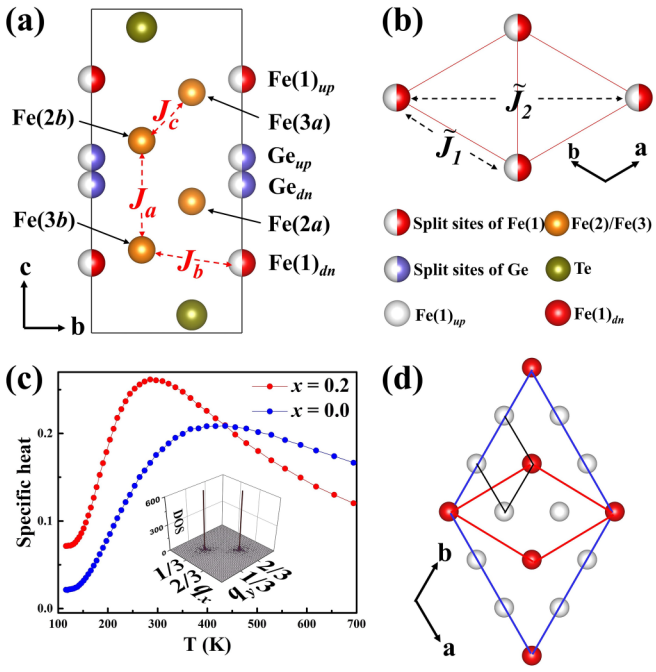

FIG. 1. (a) Average crystal structure of F5GT sublayer. The white, red, orange, blue, and dark green spheres represent Fe(1)$_{up}$, Fe(1)$_{dn}$, Fe(2)(3), Ge, and Te atoms, respectively. (b) Illustration of the Fe(1) sublattice, half white and red indicate split sites of Fe(1) on a triangular lattice. (c) Specific heat as a function of temperature simulated for $x = 0$ and $x = 0.2$. The inset depicts the analysis of the discrete Fourier transformation of the structure at 153 K for $x = 0$. (d) Schematic of the short-range ordered (SRO) superstructure. The 3×3 superstructure is marked by the blue axis with the corresponding primitive $\sqrt{3} \times \sqrt{3}$ superstructure marked by the red axis.

resemble closely that of the bulk, therefore, indicates pervasive beyond-room-temperature two-dimensional ferromagnetism.

II. LATTICE STRUCTURE

The average crystal structure of bulk F5GT has a rhombohedral space-group $R\bar{3}m$ [7] with three identical layers stacked staggeringly in each unit cell, labeled as ABC stacking. Each layer consists of a Fe_5Ge sublayer sandwiched between two Te planes as shown in Fig. 1(a). The two split sites of Fe(1) atoms are in the outermost plane of each Fe_5Ge sublayer. First-principles calculations indicate that Fe(1)$_{up}$-Ge$_{up}$ or Fe(1)$_{dn}$-Ge$_{dn}$ pairs are not allowed due to bond distance restrictions, i.e., when the Fe(1) atom occupies the up site, the corresponding Ge atom can only occupy the down site, forming Fe(1)$_{up}$-Ge$_{dn}$ or, equivalently, Fe(1)$_{dn}$-Ge$_{up}$ pairs. Interestingly, Fe(1) positions form a triangular lattice on the plane as shown in Fig. 1(b). If Fe(1)$_{up}$-Ge$_{dn}$ and Fe(1)$_{dn}$-Ge$_{up}$ pairs are viewed as spin up and spin down, respectively, the problem of Fe(1) order translates into an Ising model on a triangular lattice. The Hamiltonian of the Ising model can then be written as

$$H = \sum_{i<j} \tilde{J}_{ij} S_i S_j \quad (S_{i,j} = \pm 1), \tag{1}$$

where $\tilde{J}_i$ corresponds to the ith nearest-neighbor (NN) effective interaction between Fe(1)-Ge occupation pairs [see Fig. 1(b)]. We calculate $\tilde{J}_i$ up to the second-nearest neighbor by fitting to first-principles calculated energies, obtaining $\tilde{J}_1 = 30.2$ and $\tilde{J}_2 = 0.99$ meV for F5GT, which shows that this system is an antiferromagnetic frustrated Ising model on a triangular lattice. Such a model with only $\tilde{J}_1$ is well known for its lack of long-range order at finite temperatures with an infinitely degenerate ground state, composed of $\sqrt{3} \times \sqrt{3}$ superstructures with two up and one down spins (or, equivalently, two down and one up) on each triangle [24,25]. The additional small $\tilde{J}_2$ may break the infinite degeneracy but barely change the general behavior of the original model at the temperatures that we are concerned (see our simulations in Fig. S2 in the Supplemental Material [26]). Specific heat from re-MC simulations show a bump peaked at around 380 K, which does not become sharper with increasing lattice size (shown in Fig. S2(a) of the Supplemental Material [26]), indicating a weak size dependence and SRO structures [see Fig. 1(c) blue curve] [25]. Spectra analysis by performing discrete Fourier transformation on the structures obtained from re-MC at low temperatures shows the highest density of states locating at $q = (1/3, 1/3, 0)$ and $q = (2/3, 2/3, 0)$ [the inset of Fig. 1(c)], indicating that the SRO structures are, indeed, $\sqrt{3} \times \sqrt{3}$ superstructures, which is in good agreement with the fast Fourier transformation pattern of the high-angle annular dark-field (HAADF) images from experiments [7]. A representative superstructure from our model is shown in Fig. 1(d). Notably, the superstructure preserves the C_3 rotational symmetry of the averaged structure, exhibiting a Fe(1)$_{dn}$Fe(1)$_{up}$Fe(1)$_{up}$ (*duu*) or Fe(1)$_{up}$Fe(1)$_{dn}$Fe(1)$_{dn}$ (*udd*) order along [100], [010], and [110] directions. Our direct first-principles calculations also show that the *duu* or *udd* structures have lower energy than the *uuu* or *ddd* structures, inconsistent with the conclusions of the Ising model.

For Ni-F5GT, although the average structure with Ni doping changes from ABC stacking to AA stacking (space-group $P\bar{3}m1$) [14], the geometry of each sublayer still remains intact. Therefore, the intrinsic structural disorder induced by split sites of Fe(1) occupation persists with Ni doping with a possibility of forming similar superstructures as in F5GT. To make our computations feasible, the Ni doping is simulated by using the lowest-energy structure obtained at each corresponding Ni content in a supercell. Our calculations show that the doped Ni atoms tend to first substitute the Fe(1), then, gradually replace Fe(2) and Fe(3) with increasing Ni content. We here use Ni-F5GT with $x = 0.2$ in which case all Fe(1) atoms are replaced by Ni atoms with other Fe atoms unaffected, as an example to illustrate the potential structural ordering in Ni-F5GT. The same Ising model [Eq. (1)] can then be applied with $\tilde{J}_{ij}$ now standing for the interaction between Ni-Ge structural pairs. We obtain $\tilde{J}_1 = 17.9$, $\tilde{J}_2 = -3.2$ meV with simulated specific heat shown in Fig. 1(c) (red curve). Compared to $x = 0$, the bump of the specific heat becomes sharper with its peak position shifted to a lower temperature at around 300 K as a result of smaller $\tilde{J}$ values but a larger $\tilde{J}_2/\tilde{J}_1$ ratio, making it deviating more from a perfect triangular NN antiferromagnetic Ising model. The results of corresponding Fourier spectra analysis of Ni-F5GT with $x = 0.2$ is similar to that of F5GT, showing two peaks at $q = (1/3, 1/3, 0)$ and

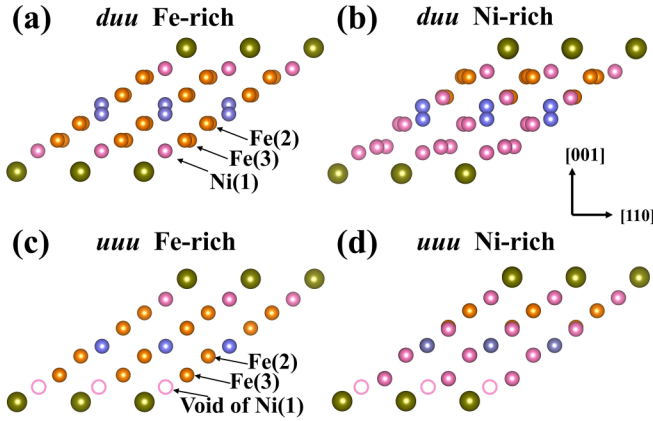

FIG. 2. Illustrations of the TGT plane structure in Ni-F5GT systems. The pink, orange, blue, and dark green spheres represent Ni, Fe, Ge, and Te atoms, respectively. The optimized *duu* structure at (a) $x = 0.2$ and (b) $x = 0.667$. The optimized *uuu* structure at (c) $x = 0.2$ and (d) $x = 0.667$.

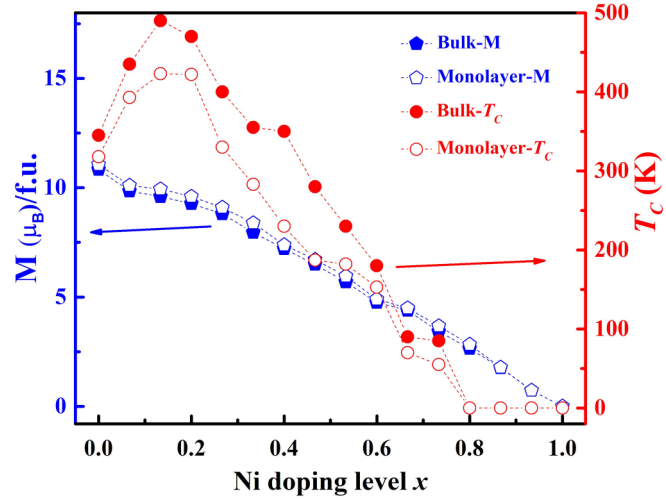

FIG. 3. Ni-doping level x-dependent magnetic moments and T_c of bulk (solid symbol) and monolayer (open symbol) Ni-F5GT systems marked by blue and red curves, respectively.

$q = (2/3, 2/3, 0)$ but with higher peak intensity, which indicates that with Ni doping, the $\sqrt{3} \times \sqrt{3}$ superstructure should also be observable (see Fig. S3 of the Supplemental Material [26]). To examine more of the structure, in each sublayer of F5GT, the sites of Fe atoms are symmetric with respect to the Ge atom at the center, forming a Te-Fe(1)-Fe(3)-Fe(2)-Ge-Fe(2)-Fe(3)-Fe(1)-Te plane (labeled as the TGT plane) [see Fig. 2(a)]. First-principles optimized $\sqrt{3} \times \sqrt{3}$ superstructure of Ni-F5GT (*duu*) with $x = 0.2$ shows a flat TGT plane [see Fig. 2(b)], whereas for $x = 0.667$, the TGT plane is rumpled, which both agree perfectly with HAADF scanning transmission electron microscopy experiments [14]. In contrast, structure optimized with the $Fe(1)_{up}Fe(1)_{up}Fe(1)_{up}$ (*uuu*) structure of Ni-F5GT cannot accommodate a complete TGT plane with the loss of one Fe(1)/Ni atom due to all Fe(1) atoms occupy the up site, further supporting the existence of the $\sqrt{3} \times \sqrt{3}$ superstructure in Ni-F5GT [see Figs. 2(c) and 2(d)]. It is, therefore, reasonable to argue that at finite temperatures, the experimental lattice structures are composed of domains with different SRO $\sqrt{3} \times \sqrt{3}$ superstructures.

III. MAGNETISM

It is straightforward to assume that magnetism of the ordered superstructure could exhibit noticeable difference from that of the *uuu* (or *ddd*) structure due to the change in local environment related to Fe(1) atoms as also suggested in Ref. [23]. We, therefore, further investigate the magnetism, first the magnetic moments **M**, using the ordered superstructure. For F5GT, Fe atoms are divided into six inequivalent positions, labeled here as $Fe(1)_{up}$, $Fe(1)_{dn}$, Fe(2*a*), Fe(2*b*), Fe(3*a*), and Fe(3*b*) [see Fig. 1(a)] with each $|\mathbf{M}|$ of the bulk calculated as 1.80, 1.88, 1.98, 2.24, 2.49, and 2.45 μ_B, respectively, which agree with the values 0.6–2.6 μ_B/Fe obtained from experiments [7]. With Ni doping, the calculated total magnetic moments $|\mathbf{M}_{tot}|$ of the bulk Ni-F5GT fall approximately linearly with the increase in doping level x, from 10.8 μ_B/f.u. at $x = 0$ to zero at $x = 1$ (see Fig. 3). The doped Ni atoms are found to be weakly magnetic with $\mathbf{M}_{Ni} \sim 0.27\ \mu_B$ at $x \leqslant 0.5$, whereas at higher doping levels, $\mathbf{M}_{Ni}$ vanishes, therefore, result in a progressive dilution of the total magnetization with the increasing in$x$. For more details, the magnetic moment at each different site decreases stagewise because of the nearly ordered substitution of each Fe site by Ni, i.e., fully replace one site before going to the next (see Fig. S6 of the Supplemental Material [26]). When it comes to the monolayer, the $|\mathbf{M}_{tot}|$ behaves similarly with that of the bulk, but have slightly larger magnitude because of enhanced localization in the low-dimensional case.

Furthermore, for F5GT, we study the change in each $|\mathbf{M}|$ by varying their relative canting angles. For instance, when the spin angle is forced from 0° (parallel to other spins) to 90° (perpendicular to other spins), $|\mathbf{M}_1|$, $|\mathbf{M}_{2a}|$, and $|\mathbf{M}_{2b}|$ are each reduced by a non-negligible 0.6 μ_B, whereas $|\mathbf{M}_{3a}|$ and $|\mathbf{M}_{3b}|$ remain nearly constant (see Fig. S4 of the Supplemental Material [26]), which indicate the coexistence of itinerant and localized magnetism in the F5GT systems with the itinerant character mainly situated on Fe(1), Fe(2*a*), and Fe(2*b*) atoms. Moreover, we calculate the total energy dependence on the variation of each $|\mathbf{M}_i|$ with results shown in Fig. 4. It can be

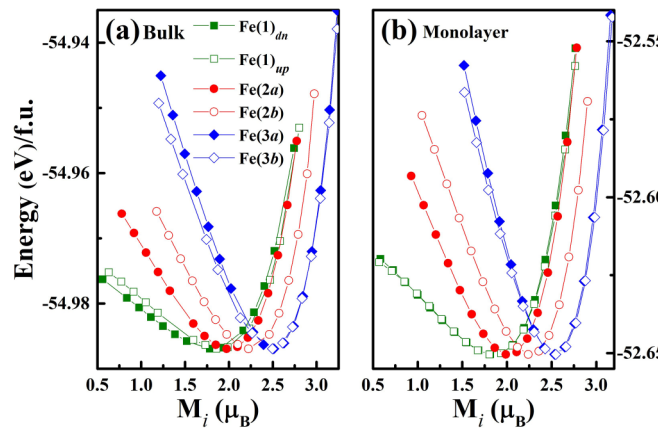

FIG. 4. $\mathbf{M}_i$-dependent energy in (a) bulk and (b) monolayer F5GT.

seen that the energy wells on $|\mathbf{M}_1|$, $|\mathbf{M}_{2a}|$, and $|\mathbf{M}_{2b}|$ are significantly asymmetric with respect to each well bottom with a flatter rising on the low moment side, typical for itinerant magnetic systems, such as bcc Fe and fcc Ni [27–30]. This could result in noticeable redistribution of relevant $|\mathbf{M}_i|$ with variation in temperature (see Fig. S10 of the Supplemental Material [26]), even lead to finite magnetic moments purely stabilized by thermal fluctuations at high temperatures. However, the energy wells on $|\mathbf{M}_{3a}|$ and $|\mathbf{M}_{3b}|$ are much deeper and nearly symmetric with respect to each well bottom, therefore, $|\mathbf{M}_{3a}|$ and $|\mathbf{M}_{3b}|$ are expected to remain localized and only exhibit negligible fluctuations in the temperature range we are interested in. When Ni doping is introduced, each remaining Fe magnetic moment largely keeps their original character. However, with only small magnetic moments around 0.27 μ_B, $\mathbf{M}_{Ni}$ is also expected to be strongly itinerant (see Figs. S5 and S6 of the Supplemental Material [26]).

To describe simultaneously the localized and itinerant magnetism in the F5GT systems, we resort to the Heisenberg-Landau Hamiltonian [27–30],

$$H = \sum_{i<j} J_{ij}\mathbf{M}_i \cdot \mathbf{M}_j - \sum_i D\left(\mathbf{M}_i^z\right)^2 + \sum_i A_i\mathbf{M}_i^2 + \sum_i B_i\mathbf{M}_i^4 + \sum_i C_i\mathbf{M}_i^6, \quad (2)$$

where the first two terms represent Heisenberg exchange interactions with single-ion anisotropy and the rest correspond to the Landau expansion terms, taking into account the longitudinal fluctuation of magnetic moments. For simplicity, we choose J_{ij} to be $\mathbf{M}$ independent and the Landau terms are expanded to the sixth order. The expansion coefficients A, B, and C are only considered for magnetic moments with noticeable itinerant characters, $|\mathbf{M}_1|$, $|\mathbf{M}_{2a}|$, $|\mathbf{M}_{2b}|$, and $|\mathbf{M}_{Ni}|$. For $\mathbf{M}_{Ni}$, an 8th term $\sum_i D_i\mathbf{M}_{Ni}^8$ is also added for a better fit. The J's are then calculated using the TB2J code [31] and the expansion coefficients are calculated by fitting to first-principles constrained magnetic moment calculations with obtained results shown in Tables S2–S5 (see the details in the Supplemental Material [26], see, also Refs. [32–39] therein). Re-MC simulations are then performed to study phase diagram of this Hamiltonian. Only single phase transitions from paramagnetic (PM) phases to FM phases are obtained with T_c of bulk and monolayer F5GT at about 345 and 318 K, respectively, which are slightly higher than experimental values 279–332 K for bulk and 280–300 K for the monolayer [7,10–12]. It is worth noting that experimental samples of F5GT all have noticeable Fe deficiencies, which could lead to lower T_c compared to simulations on perfect crystals. Surprisingly, the longitudinal spin fluctuations are found to only affect the T_c's mildly with a modification of ∼5% with respect to that obtained with standard Heisenberg interactions (see Fig. S9 of the Supplemental Material [26]), less significant than the ∼10% lowering revealed for bcc Fe [27]. This rather weak effect from the Landau terms is due to that only part of the Fe magnetism can be considered itinerant and the dominant FM exchange interactions are not heavily affected. Notably, our calculations on bulk Ni-F5GT also show that a light Ni doping can enhance the T_c, up to 490 K at $x = 0.2$ and then slowly reduce the T_c, down to zero when $x > 0.8$, exhibiting

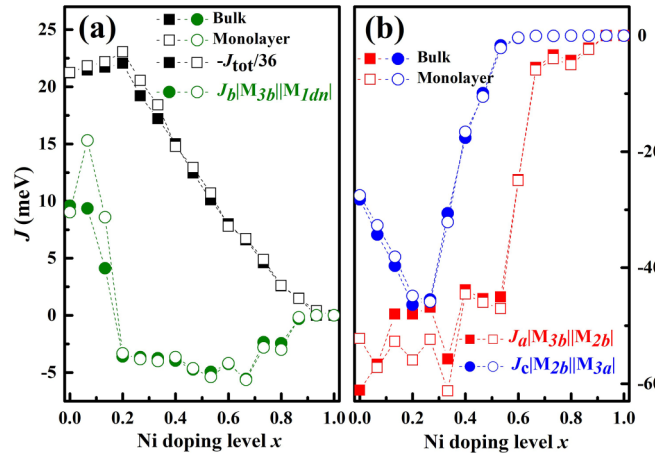

FIG. 5. The major exchange interactions of bulk (solid symbol) and monolayer (open symbol) of Ni-F5GT as a function of Ni-doping level x.

overall behavior in good agreement with recent experimental observations [14]. Moreover, our simulations show that at low doping levels, T_c of monolayer Ni-FGT is only slightly lower that its counterpart of the bulk, indicating pervasive ferromagnetism in 2D Ni-F5GT.

We now look into the calculated J_{ij} to explore the underlying mechanism behind the tuning of T_c by Ni doping. As a first step, we look at the sum of all J's with $J_{tot} = \frac{1}{2}\sum_{ij} J_{ij}|\mathbf{M}_i||\mathbf{M}_j|$, which is roughly proportional to T_c on the mean field level. Not out of expectation, it can be seen that J_{tot} is strongly negative with its absolute values following the same trend with Ni doping as that of the calculated T_c [Fig. 5(a)]. When moderate Ni doping is introduced($0 \leqslant x \leqslant 0.53$), the strongest intralayer interaction $J_a|\mathbf{M}_{2b}||\mathbf{M}_{3b}|$ [marked in Fig. 1(a)] remains ferromagnetic (−45 to −60 meV), providing dominant contribution to stabilize the FM phase. As aforementioned, under light Ni doping with $x \leqslant 0.2$, only Fe(1) is substituted, therefore, in this case, exchange interactions related to Fe(1) affect the tuning of T_c directly. In the case of zero doping, the exchange interactions related to Fe(1) are frustrated with AFM interactions between Fe(1) and its nearest Fe($3b$)($J_b|\mathbf{M}_{3b}||\mathbf{M}_{1dn}| =$ 9.6 meV), but stronger FM interactions between Fe(1) and Fe($2a$) ($J_{1,2a}|\mathbf{M}_{1dn}||\mathbf{M}_{2a}| = -24.66$ meV), therefore, Fe(1) is forced to be parallel to Fe($2a$) to stabilize the FM state. A light Ni doping replaces the original magnetic moment of Fe(1)(∼1.8 μ_B) by smaller M_{Ni}(∼ 0.27 μ_B), resulting in a decrease in average AFM J_b, which even become FM with $x \geqslant 0.2$. On the other hand, as shown in Fig. 5(b), the overall strength of FM $J_c|\mathbf{M}_{2b}||\mathbf{M}_{3a}|$ is greatly promoted from −28 to −48 meV at $0 \leqslant x \leqslant 0.2$. This cooperative weakening of AFM J_b and the enhancement of FM J_c, thus, play the pivotal role to increase the T_c at low doping level. However, further Ni doping can dilute major FM couplings [see Fig. 5(b)], leading to the decrease in T_c.

For comparison, we also investigate magnetism of F5GT and Ni-F5GT using the *uuu* structure with calculated magnetic moments and T_c shown in Fig. S11 of the Supplemental Material [26]. In this case, the magnetic moments of Fe(1)

vanish. Therefore, with light Ni doping, the saturated magnetic moments are calculated to rise first and then decrease, in qualitative variation with the monotonous decreasing behavior of corresponding experimental results. Although Curie temperatures are calculated to be similarly enhanced under low level doping but is up to 525 K at $x = 0.2$, which is much higher than the experimental values. It is worth emphasizing that our focus in this paper, is on the itinerant magnetism and T_c, other than the seemingly intricate phase diagrams observed below T_c in experiments, which may well be related to weak but subtle interlayer interactions since a tiny Ni doping induced structural transition from ABC stacking to AA stacking can completely smear the complexity out and bring the phase diagram to a simple single PM to FM transition (see Ref. [14]). To capture these subtle interactions may be beyond the current capabilities of standard *ab initio* calculations and beyond the scope of this paper, we, thus, leave it to future studies.

To summarize, we propose an antiferromagnetic Ising model on a triangular lattice, based on first-principles calculations, to interpret the ordering of Fe(1) atoms and the formation of the $\sqrt{3} \times \sqrt{3}$ superstructures in F5GT. Similar superstructures are then predicted to exist in Ni-F5GT. Our study suggests that F5GT systems may be considered as a rare structural realization of the well-known antiferromagnetic Ising model on a triangular lattice. Based on the superstructures, a Heisenberg-Landau Hamiltonian, taking into account longitudinal spin fluctuations, is implemented to study the magnetic properties of F5GT and Ni-F5GT. We unveil that frustrated magnetic interactions associated with Fe(1), tuned by a tiny Ni doping, is responsible for the experimentally observed significant enhancement of the T_c in Ni-F5GT. In contrast, calculated results based on the *uuu* structure deviate qualitatively from experiments. Itinerant magnetism, reflected by longitudinal spin fluctuations, are found to only affect the T_c's mildly with a modification of ∼5% with respect to that obtained with standard Heisenberg interactions. Our calculations further show that at low doping levels, the magnetic behaviors of the monolayer Ni-F5GT resemble closely that of the bulk, therefore, indicates pervasive beyond-room-temperature two-dimensional ferromagnetism.

ACKNOWLEDGMENTS

Work at Sun Yat-Sen University was supported by the National Key Research and Development Program of China (Grants No. 2018YFA0306001 and No. 2017YFA0206203), and the Guangdong Basic and Applied Basic Research Foundation (Grants No. 2022A1515011618 and No. 2019A1515011337), and the National Natural Science Foundation of China (Grants No. 92165204 and No. 11974432) Shenzhen International Quantum Academy (Grant No. SIQA202102), Leading Talent Program of Guangdong Special Projects (Grant No. 201626003).

[1] C. Gong, L. Li, Z. Li, H. Ji, A. Stern, Y. Xia, T. Cao, W. Bao, C. Wang, Y. Wang, Z. Q. Qiu, R. J. Cava, S. G. Louie, J. Xia, and X. Zhang, Discovery of intrinsic ferromagnetism in two-dimensional van der Waals crystals, Nature (London) **546**, 265 (2017).

[2] B. Huang, G. Clark, E. Navarro-Moratalla, D. R. Klein, R. Cheng, K. L. Seyler, D. Zhong, E. Schmidgall, M. A. McGuire, D. H. Cobden, W. Yao, D. Xiao, P. Jarillo-Herrero, and X. Xu, Layer-dependent ferromagnetism in a van der Waals crystal down to the monolayer limit, Nature (London) **546**, 270 (2017).

[3] D. C. Freitas, R. Weht, A. Sulpice, G. Remenyi, P. Strobel, F. Gay, J. Marcus, and M. Núñez-Regueiro, Ferromagnetism in layered metastable $1T$-$CrTe_2$, J. Phys.: Condens. Matter **27**, 176002 (2015).

[4] X. Sun, W. Li, X. Wang, Q. Sui, T. Zhang, Z. Wang, L. Liu, D. Li, S. Feng *et al.*, Room temperature ferromagnetism in ultra-thin van der Waals crystals of 1T-$CrTe_2$, Nano Res. **13**, 3358 (2020).

[5] Y. Deng, Y. Yu, Y. Song, J. Zhang, N. Z. Wang, Z. Sun, Y. Yi, Y. Z. Wu, S. Wu, J. Zhu *et al.*, Gate-tunable room-temperature ferromagnetism in two-dimensional Fe_3GeTe_2, Nature (London) **563**, 94 (2018).

[6] J. Seo, D. Y. Kim, E. S. An, K. Kim, G.-Y. Kim, S.-Y. Hwang, D. W. Kim *et al.*, Nearly room temperature ferromagnetism in a magnetic metal-rich van der Waals metal, Sci. Adv. **6**, eaay8912 (2020).

[7] A. F. May, D. Ovchinnikov, Q. Zheng, R. Hermann, S. Calder, B. Huang, Z. Fei, Y. Liu, X. Xu, and M. A. McGuire, Ferromagnetism near room temperature in the cleavable van der Waals crystal Fe_5GeTe_2, ACS Nano **13**, 4436 (2019).

[8] J. Stahl, E. Shlaen, and D. Johrendt, The van der Waals ferromagnets $Fe_{5-\delta}GeTe_2$ and $Fe_{5-x-\delta}Ni_xGeTe_2$crystal structure, stacking faults, and magnetic properties, Z. Anorg. Allg. Chem **644**, 1923 (2018).

[9] Z.-X. Shen, X. Bo, K. Cao, X. Wan, and L. He, Magnetic ground state and electron-doping tuning of Curie temperature in Fe_3GeTe_2: First-principles studies, Phys. Rev. B **103**, 085102 (2021).

[10] H. Zhang, R. Chen, K. Zhai, X. Chen, L. Caretta, X. Huang, R. V. Chopdekar, J. Cao, J. Sun, J. Yao, R. Birgeneau, and R. Ramesh, Itinerant ferromagnetism in van der Waals $Fe_{5-x}GeTe_2$ crystals above room temperature, Phys. Rev. B **102**, 064417 (2020).

[11] L. Alahmed, B. Nepal, J. Macy, W. Zheng, B. Casas, A. Sapkota *et al.*, Magnetism and spin dynamics in room-temperature van der Waals magnet $Fe_{5-x}GeTe_2$, 2D Mater. **8**, 045030 (2021).

[12] H. Chen, S. Asif, M. Whalen, J. Támara-Isaza, B. Luetke, Y. Wang, X. Wang, M. Ayako, S. Lamsal, A. F. May, M. A. McGuire, C. Chakraborty, J. Q. Xiao, and M. J. H. Ku, Revealing room temperature ferromagnetism in exfoliated Fe_5GeTe_2 flakes with quantum magnetic imaging, 2D Mater. **9**, 025017 (2022).

[13] A. F. May, J. Yan, R. Hermann, M.-H. Du, and M. A. McGuire, Tuning the room temperature ferromagnetism in Fe_5GeTe_2 by arsenic substitution, 2D Mater. **9**, 015013 (2022).

[14] X. Chen, Y.-T. Shao, R. Chen, S. Susarla, T. Hogan, Y. He, H. Zhang, S. Wang, J. Yao, P. Ercius, D. A. Muller, R. Ramesh, and R. J. Birgeneau, Pervasive beyond Room-Temperature Ferromagnetism in a Doped van der Waals Magnet, Phys. Rev. Lett. **128**, 217203 (2022).

[15] H. Zhang, D. Raftrey, Y.-T. Chan, Y.-T. Shao, R. Chen, X. Chen, X. Huang, J. T. Reichanadter, K. Dong, S. Susarla, L. Caretta, Z. Chen, J. Yao, P. Fischer, J. B. Neaton, W. Wu, D. A. Muller, R. J. Birgeneau, and R. Ramesh, Room-temperature skyrmion lattice in a layered magnet $Fe_{0.5}Co_{0.5}GeTe_2$, Sci. Adv. **8**, eabm7103 (2022).

[16] H. Zhang, Y.-T. Shao, R. Chen, X. Chen, S. Susarla, D. Raftrey, J. T. Reichanadter, L. Caretta, X. Huang, N. S. Settineri, Z. Chen, J. Zhou, E. Bourret-Courchesne, P. Ercius, J. Yao, P. Fischer, J. B. Neaton, D. A. Muller, R. J. Birgeneau, and R. Ramesh, A room temperature polar magnetic metal, Phys. Rev. Mater. **6**, 044403 (2022).

[17] M. Joe, U. Yang, and C. Lee, First-principles study of ferromagnetic metal Fe_5GeTe_2, Nano Mater. Sci. **1**, 299 (2019).

[18] C. Tan, W.-Q. Xie, G. Zheng, N. Aloufi, S. Albarakati, M. Algarni, J. Li, J. Partridge, D. Culcer, X. Wang, J. B. Yi, M. Tian, Y. Xiong, Y.-J. Zhao, and L. Wang, Gate-controlled magnetic phase transition in a van der Waals magnet Fe_5GeTe_2, Nano Lett. **21**, 5599 (2021).

[19] Q. Liu, J. Xing, Z. Jiang, Y. Guo, X. Jiang, Y. Qi, and J. Zhao, Layer-dependent magnetic phase diagram in $Fe_nGeTe_2(3 \leqslant n \leqslant 7)$ ultrathin films, Commun. Phys. **5**, 140 (2022).

[20] X. Yang, X. Zhou, W. Feng, and Y. Yao, Strong magneto-optical effect and anomalous transport in the two-dimensional van der Waals magnets $Fe_nGeTe_2(n = 3, 4, 5)$, Phys. Rev. B **104**, 104427 (2021).

[21] T. T. Ly, J. Park, K. Kim, H.-B. Ahn, N. J. Lee, K. Kim, T.-E. Park, G. Duvjir, N. H. Lam, K. Jang, C.-Y. You, Y. Jo, S. K. Kim, C. Lee, S. Kim, and J. Kim, Direct observation of Fe-Ge ordering in $Fe_{5-x}GeTe_2$ crystals and resultant helimagnetism, Adv. Funct. Mater. **31**, 2009758 (2021).

[22] X. Wu, L. Lei, Q. Yin, N.-N. Zhao, M. Li, Z. Wang, Q. Liu, W. Song, H. Ma, P. Ding, Z. Cheng, K. Liu, H. Lei, and S. Wang, Direct observation of competition between charge order and itinerant ferromagnetism in the van der Waals crystal $Fe_{5-x}GeTe_2$, Phys. Rev. B **104**, 165101 (2021).

[23] S. Ershadrad, S. Ghosh, D. Wang, Y. Kvashnin, and B. Sanyal, Unusual magnetic features in two-dimensional $Fe_{5-x}GeTe_2$ induced by structural reconstructions, J. Phys. Chem. Lett. **13**, 4877 (2022).

[24] G. H. Wannier, Antiferromagnetism. The Triangular Ising net, Phys. Rev. **79**, 357 (1950).

[25] Y. Saito and K. Igeta, Antiferromagnetic Ising Model on a Triangular Lattice, J. Phys. Soc. Jpn. **53**, 3060 (1984).

[26] See Supplemental Material at http://link.aps.org/supplemental/10.1103/PhysRevB.106.224423 for computational details and some additional results, including the exchange interactions, expansion coefficients, etc.

[27] P.-W. Ma and S. L. Dudarev, Longitudinal magnetic fluctuations in Langevin spin dynamics, Phys. Rev. B **86**, 054416 (2012).

[28] A. V. Ruban, S. Khmelevskyi, P. Mohn, and B. Johansson, Temperature-induced longitudinal spin fluctuations in Fe and Ni, Phys. Rev. B **75**, 054402 (2007).

[29] N. M. Rosengaard and B. Johansson, Finite-temperature study of itinerant ferromagnetism in Fe, Co, and Ni, Phys. Rev. B **55**, 14975 (1997).

[30] M. Uhl and J. Kübler, Exchange-Coupled Spin-Fluctuation Theory: Application to Fe, Co, and Ni, Phys. Rev. Lett. **77**, 334 (1996).

[31] X. He, N. Helbig, M. J. Verstraete, and E. Bousquet, TB2J: A python package for computing magnetic interaction parameters, Comput. Phys. Commun. **264**, 107938 (2021).

[32] G. Kresse and J. Hafner, *Ab initio* molecular dynamics for liquid metals, Phys. Rev. B **47**, 558 (1993).

[33] P. E. Blöchl, Projector augmented-wave method, Phys. Rev. B **50**, 17953 (1994).

[34] G. Kresse and J. Furthmüller, Efficient iterative schemes for *ab initio* total-energy calculations using a plane-wave basis set, Phys. Rev. B **54**, 11169 (1996).

[35] J. P. Perdew, K. Burke, and M. Ernzerhof, Generalized Gradient Approximation Made Simple, Phys. Rev. Lett. **77**, 3865 (1996).

[36] S. Grimme, J. Antony, S. Ehrlich, and H. Krieg, A consistent and accurate *ab initio* parametrization of density functional dispersion correction (DFT-D) for the 94 elements H-Pu, J. Chem. Phys. **132**, 154104 (2010).

[37] G. Pizzi, V. Vitale, R. Arita, S. Blügel, F. Freimuth, G. Géranton, M. Gibertini, D. Gresch, C. Johnson, T. Koretsune, J. Ibañez-Azpiroz, H. Lee, J.-M. Lihm, D. Marchand, A. Marrazzo, Y. Mokrousov, J. I. Mustafa, Y. Nohara, Y. Nomura, L. Paulatto *et al.*, Wannier90 as a community code: New features and applications, J. Phys.: Condens. Matter **32**, 165902 (2020).

[38] N. Marzari and D. Vanderbilt, Maximally localized generalized Wannier functions for composite energy bands, Phys. Rev. B **56**, 12847 (1997).

[39] I. Souza, N. Marzari, and D. Vanderbilt, Maximally localized Wannier functions for entangled energy bands, Phys. Rev. B **65**, 035109 (2001).

Correction: An error in a grant number in the Acknowledgment section was introduced during the proof production cycle and has been fixed.